iScience

CellPress
OPEN ACCESS

Article

Helically arranged cross struts in azhdarchid pterosaur cervical vertebrae and their biomechanical implications

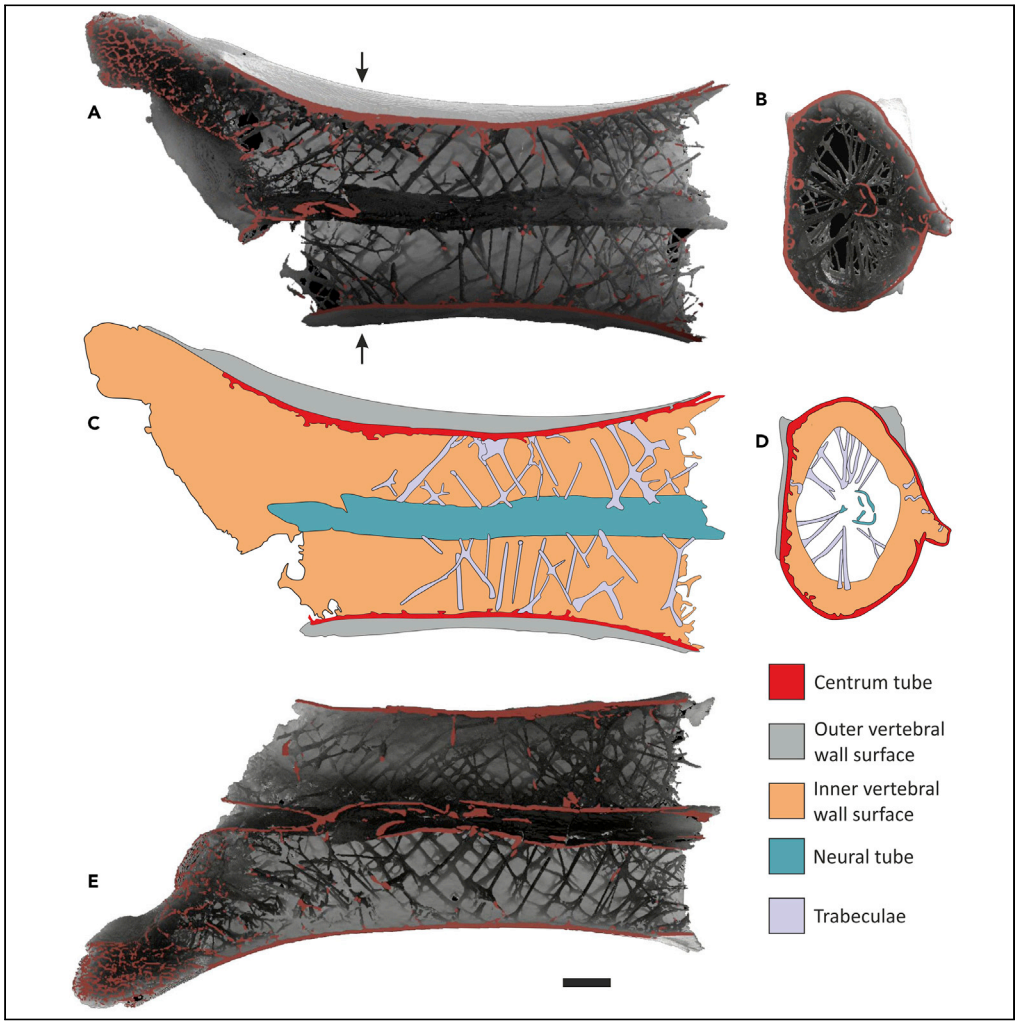

Cariad J. Williams, Martino Pani, Andrea Bucchi, ..., William Keeble, Nizar Ibrahim, David M. Martill

david.martill@port.ac.uk

Highlights

Trabeculae in a pterosaur cervical vertebra are helically arranged.

As few as 50 trabeculae increase the buckling load by up to 90%.

Subsuming the neural tube into the centrum adds stiffness to the cervical series.

Williams et al., iScience *24*, 102338
April 23, 2021
https://doi.org/10.1016/j.isci.2021.102338

iScience

CellPress
OPEN ACCESS

Article

Helically arranged cross struts in azhdarchid pterosaur cervical vertebrae and their biomechanical implications

Cariad J. Williams,[1,2,7] Martino Pani,[3] Andrea Bucchi,[3] Roy E. Smith,[1] Alexander Kao,[4,5] William Keeble,[6] Nizar Ibrahim,[1] and David M. Martill[1,*]

SUMMARY

Azhdarchid pterosaurs, the largest flying vertebrates, remain poorly understood, with fundamental aspects of their palaeobiology unknown. X-ray computed tomography reveals a complex internal micro-architecture for three-dimensionally preserved, hyper-elongate cervical vertebrae of the Cretaceous azhdarchid pterosaur, *Alanqa* sp. Incorporation of the neural canal within the body of the vertebra and elongation of the centrum result in a "tube within a tube" supported by helically distributed trabeculae. Linear elastic static analysis and linearized buckling analysis, accompanied with a finite element model, reveal that as few as 50 trabeculae increase the buckling load by up to 90%, implying that a vertebra without the trabeculae is more prone to elastic instability due to axial loads. Subsuming the neural tube into the centrum tube adds considerable stiffness to the cervical series, permitting the uptake of heavy prey items without risking damage to the cervical series, while at the same time allowing considerable skeletal mass reduction.

INTRODUCTION

Pterosaurs, volant reptiles of the Mesozoic made their first appearance in the fossil record in the Late Triassic and survived until the end of the Cretaceous approximately 66 million years ago (Unwin, 2005; Witton, 2013; Longrich et al., 2018). Although some pterosaurs were small, with wingspans of less than 1 m, the enigmatic Azhdarchidae achieved wingspans of up to 10 m, possibly even as high as 12 m (Lawson, 1975; Frey and Martill, 1996; Buffetaut et al., 2003; Witton and Habib, 2010). These gigantic forms were globally distributed, but mainly restricted to the late Early to end Late Cretaceous (Averianov, 2010, 2013; Naish and Witton, 2017). The Azhdarchidae are notable for elongation of the neck as a result of hyper-elongation of their cervical vertebrae (Frey and Martill, 1996; Unwin and Lü, 1997; Martill et al., 1998; Company et al., 1999; Unwin, 2003; Henderson and Peterson, 2006; Watabe et al., 2009; Witton, 2013; Liu et al., 2015; Harrell et al., 2016). Their cervical vertebrae (Figure 1) display many modifications of the centrum, neural arch, and articulatory facets and processes (condyles, cotyles, and zygapophyses), many of which appear to be adaptations for holding the neck in an outstretched position (Averianov, 2013; Naish and Witton, 2017). Numerous bone locks restrict flexion in three planes, and deep ligament sockets anteriorly and posteriorly imply strong linkage between individual vertebrae. Flattening of the condyle and cotyle also limits flexion to a single plane (Averianov, 2013). However, the function and complexity of the internal structure of these highly unusual vertebrae has never previously been investigated. Previous analysis of the biomechanics of azhdarchid cervical vertebrae (e.g., Averianov, 2013; Naish and Witton, 2017) modeled them as a simple, single hollow tube, but such analyses fail to correctly determine the biomechanical properties of the pterosaur neck skeleton by ignoring its internal structure. This lack of quantifiable analysis has hampered efforts to assess fundamental aspects of azhdarchid ecology, such as their prey size and neck strength.

Studies of pterosaur skeletal anatomy are often limited by a shortage of high-quality specimens displaying 3D morphology, and this is especially true for the pterosaur neck skeleton. The limited amount of morphological data for Azhdarchidae contributes to our poor understanding of the biomechanics and palaeoecology of these pterosaurs. Although three-dimensionally preserved pterosaur bones are rare, and articulated material rarer still, the mid Cretaceous Kem Kem Group of Morocco is becoming increasingly important as

[1]School of the Environment, Geography and Geosciences, University of Portsmouth, Burnaby Building, Burnaby Road, Portsmouth, PO1 3QL, UK

[2]Center for Paleontology, Illinois Natural History Survey, Prairie Research Institute, University of Illinois at Urbana-Champaign, Forbes Natural History Building 1816 S. Oak Street, Champaign, IL 61820, USA

[3]School of Mechanical and Design Engineering, University of Portsmouth, Anglesea Building, Anglesea Road, Portsmouth PO1 3DJ, UK

[4]School of Engineering, University of Portsmouth, Portland Building, Portland Street, PO1 3DJ, Portsmouth, UK

[5]Elettra Synchrotron Trieste, Science Park, 34149 Basovizza TS, Italy

[6]Faculty of Technology, University of Portsmouth, Anglesea Building, Anglesea Road, Portsmouth PO1 3DJ, UK

[7]Lead contact

*Correspondence: david.martill@port.ac.uk

https://doi.org/10.1016/j.isci.2021.102338

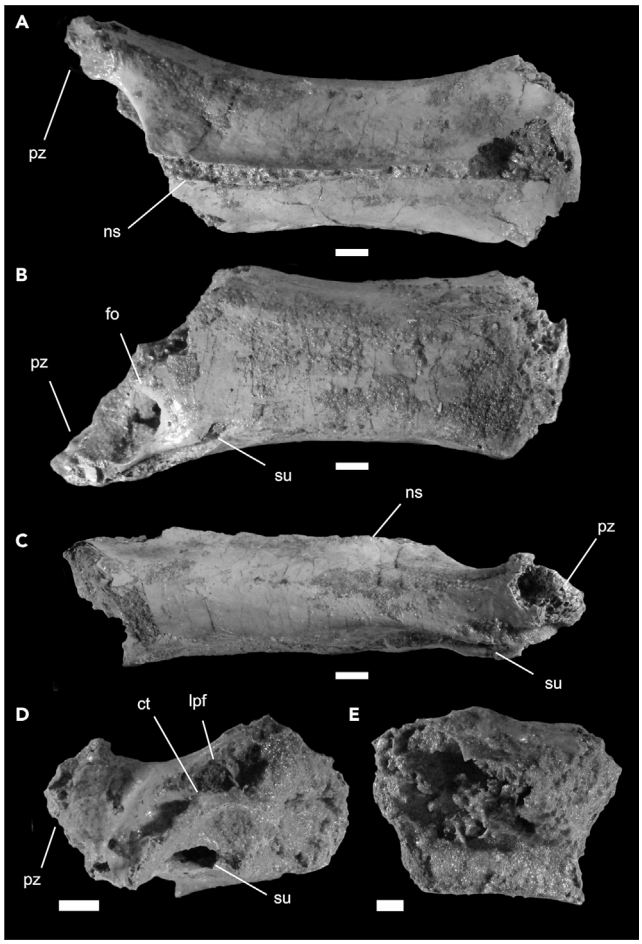

Figure 1. Cervical vertebra of *Alanqa* sp. from the Kem Kem Group of Morocco

Cervical vertebra of *Alanqa* sp. FSAC-KK 5077 in (A), dorsal view, (B), ventral view, (C), right lateral view, (D), anterior view, (E), posterior view. Scale bars represent 10 mm. Abbreviations: pz, prezygapophysis; ct, cotyle; ns, neural spine; su, sulci; fo, foramina; lpf, lateral pneumatic foramina (See Table S1 for measurements).

a source of well-preserved, 3D pterosaur bones, including azhdarchid cervical vertebrae (Ibrahim et al., 2020).

XCT scanning of a well-preserved azhdarchid cervical vertebra from the Kem Kem Group provides a rare opportunity to investigate the internal architecture of these highly derived bones to determine their mechanical properties and tolerance. We tentatively attribute these vertebrae to the taxon, *Alanqa* sp. Ibrahim et al. (2010), although we note, based on recently described finds that other azhdarchoid taxa were present in the Kem Kem Group (Ibrahim et al., 2020). The Kem Kem Group records a complex fluvial system dominated by red-bed strata. They are famous for the high abundance of fragmentary, but well-preserved remains of disarticulated vertebrates (Lavocat, 1954; Sereno et al., 1996; Ibrahim et al., 2010). Most pterosaur material has been collected from the Albian-Cenomanian Ifezouane Formation (Ibrahim et al., 2020).

Pterosaur bone

Pterosaur bones are typically hollow and usually thin walled with reduced internal trabeculae, except at points of articulation (Witton, 2013). Like all tetrapod bones, pterosaur bone is rich in osteocyte lacunae with dense fringes of canaliculae (de Ricqlès et al., 2000; Steel, 2008) and micro-capillaries, which may render the bone less dense than if it were solid (supplemental information Figure S1). Thus, pneumatized pterosaur bones likely are extremely light (Witton and Habib, 2010, but see Butler et al., 2009; Dumont, 2010; Martin and Palmer, 2014 for a discussion on the effects on pneumaticity on bone density in volant

tetrapods). Most Cretaceous pterosaur bones appear extremely fragile due to the highly reduced thickness of their bone walls (Bennett, 1997). Paleohistological studies reveal thin-walled pterosaur bone to be composed of microlamellar bone, with many lamellae per mm of thickness (de Ricqlès et al., 2000; Steel, 2008). Such histology is widely thought to confer stiffness and resist impact fracture (de Ricqlès et al., 2000).

Pterosaur neck skeleton

Pterodactyloid pterosaur necks are comparatively large structures with generally eight or nine cervical vertebrae, most of which are larger than individual thoracic, lumbar, sacral, and caudal vertebrae (Howse, 1986; Wellnhofer, 1991; Witton, 2013; Bennett, 2014). The neck is usually longer than the torso and often supports an extremely large but lightly constructed skull (Kellner and Langston, 1996). Individual vertebrae are usually pneumatized with enlarged lateral foramina, low, or even absent neural spines and in many cases are approximately as high as they are wide and long (approximately equant) (Butler et al., 2009; Claessens et al., 2009). They are procoelous and articulate with adjacent vertebrae via a horizontally oval condyle and cotyle, with inclined facets of the anterior and posterior zygapophyses (Howse, 1986; Witton, 2013).

In ctenochasmatid and azhdarchid pterosaurs cervical vertebrae are more elongate in the central portion (C3 to C7), and in Azhdarchidae, they are highly elongate and even hyper-elongate in the case of cervical five (C5) (the Romanian *Hatzegopteryx* may have secondarily shortened their neck length, but the evidence is equivocal) (Vremir et al., 2015; Naish and Witton, 2017). Most notably, the late Cretaceous azhdarchid *Arambourgiania* has a cervical vertebra (C5) with an estimated maximum length of 770 mm (Frey and Martill, 1996) and an estimated total neck length of ~2.5 m. Such elaborate structures have become the subject of several biomechanical and functional studies (Witton and Habib, 2010; Averianov, 2013; Naish and Witton, 2017), as such long necks are remarkable for volant animals. Besides their increased length, several other features distinguish azhdarchid cervical vertebrae from other pterosaurs. Notable is the lack of pneumatic foramina on the centrum sides, the reduction of the neural spine, and subsuming of the neural canal into the middle of the centrum to form a neural tube (Frey and Martill, 1996), although this latter feature has also been recorded for another group, the Dsungaripteridae (Buffetaut and Kuang, 2010).

In this analysis we examine the role of the internal architecture of an azhdarchid cervical vertebra to determine its biomechanical properties regarding azhdarchid pterosaur feeding behavior (see supplemental information for methods, Figures S2 and S3).

RESULTS

Internal architecture

The results of XCT scanning and 3D manipulation reveal a complex internal architecture of the azhdarchid cervical vertebra. Clearly visible is an approximately centrally located bony neural tube attached to the centrum wall (centrum tube) by helically arranged radial, spoke-like trabeculae (Figure 2. See also Videos S1 and S2). These are arranged as complimentary opposed helices (clockwise vs anticlockwise) and are often fused where they cross over. Superficially, looking along the length of the centrum internally the radial trabeculae resemble bicycle wheel spokes (Figures 2B and 2D). The arrangement is somewhat irregular and so the helices are not perfect, but this likely reflects changes in the stress regime along a centrum that is not a perfect cylinder. The "spokes" are inclined posteriorly or anteriorly, while still displaying the radial architecture (Figures 2B and 2D). Some "spokes" bifurcate and branch, especially toward the centrum outer wall (Figure 2A, 2C, and 2E). Toward the dorsal part of the centrum (neural arch) and the prezygapophyses the trabeculae are more densely arranged and are orientated more randomly (Figure 2A, 2C, and 2E). Trabeculae are also present along the interior wall of the vertebra, presumably providing support and increasing its strength. The "spokes" have varying diameters, with an average of 1.16 mm.

Biomechanical properties of a single cervical vertebra

The load multiplier associated with buckling changes with the number of trabeculae, because an increase in trabeculae creates a stronger bond between the external and internal tubes and increases the overall resistance of the structure to buckling (Figure 3A). An increase in trabeculae reinforces the structure by increasing its elastic stability (i.e. a bigger load to produce buckling); at the same time, this produces a stress transfer between the external bone wall and the internal neural tube (see Figure 4), thus reducing the safety factor with respect to tissue failure. In other words, with more trabeculae the structure is more

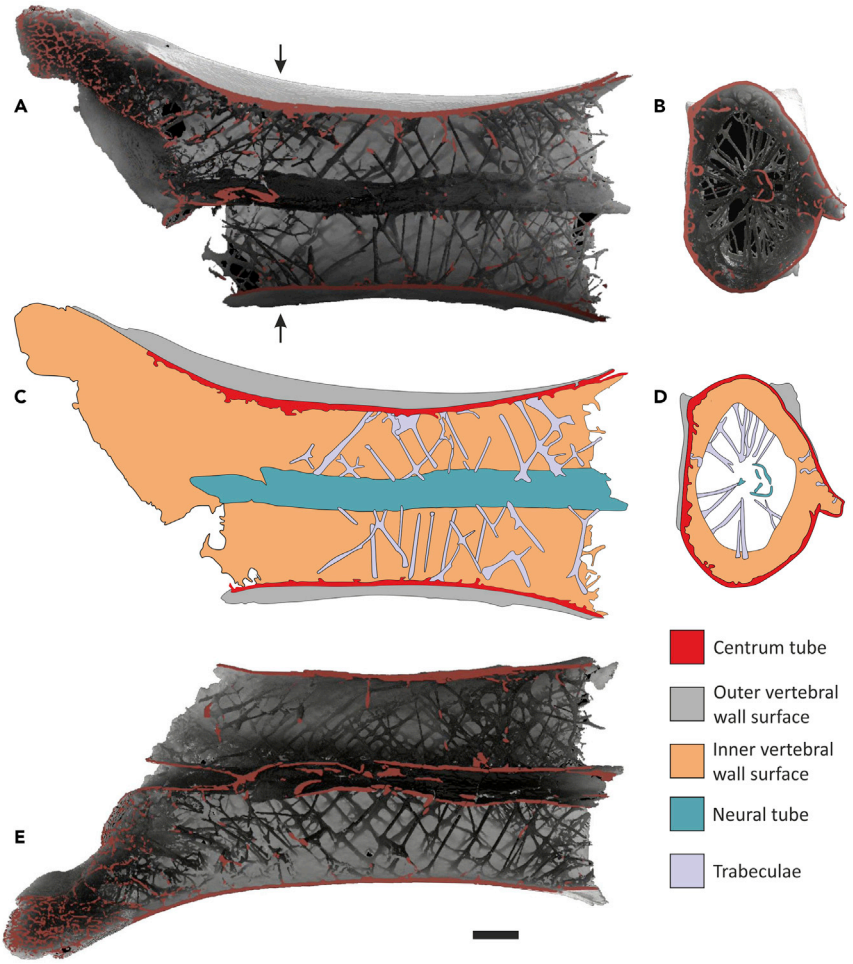

Figure 2. Images of XCT scan of cervical vertebra of *Alanqa* sp

Images of digital model generated from XCT scans of cervical vertebra FSAC-KK 5077 showing the internal architecture (A and B) and simplification diagrams of the internal structure (C and D), dorsal (A (above neural canal), (C and E) (cut through neural canal)) and anterior (B and D) views cut transversely through the cervical (position indicated by arrows). All views to same scale; scale bar represents 10 mm.

stable but closer to the limit of fracture of the material. In this sense, an optimal trade-off in the trabecula number seems to optimize the first effect (stability) with lesser impact on the latter (safety factor with respect to fracture).

The critical load triggering the structural instability shows a highly non-linear dependence with the number of trabeculae. Assuming as reference the case of no trabeculae, the critical load able to trigger buckling is increased on average up to 90% when the first 50 trabeculae are randomly introduced on the vertebral body. Conversely, the introduction of a further 400 trabeculae increased the critical load by only 10% with respect to the initial condition. Thus, when the number of trabeculae increases, the stability of the structure also increases and is less prone to buckling (i.e., the load triggering buckling increases); at the same time, the connection between the external bone wall and the internal neural tube increases, resulting in a greater tensile strain on the wall of the neural tube. Thus, as few as 50 trabeculae produce a considerable increase in the vertebra's structural stability without generating a hazardous strain concentration on the central neural tube.

Figure 3B shows the change of safety factor related to material fracture with the number of trabeculae; the chart reports the change rate with respect to the reference condition of no trabeculae. As well as the buckling load multiplier, the safety factor (i.e., how close the structure is to localized material fracture) changed

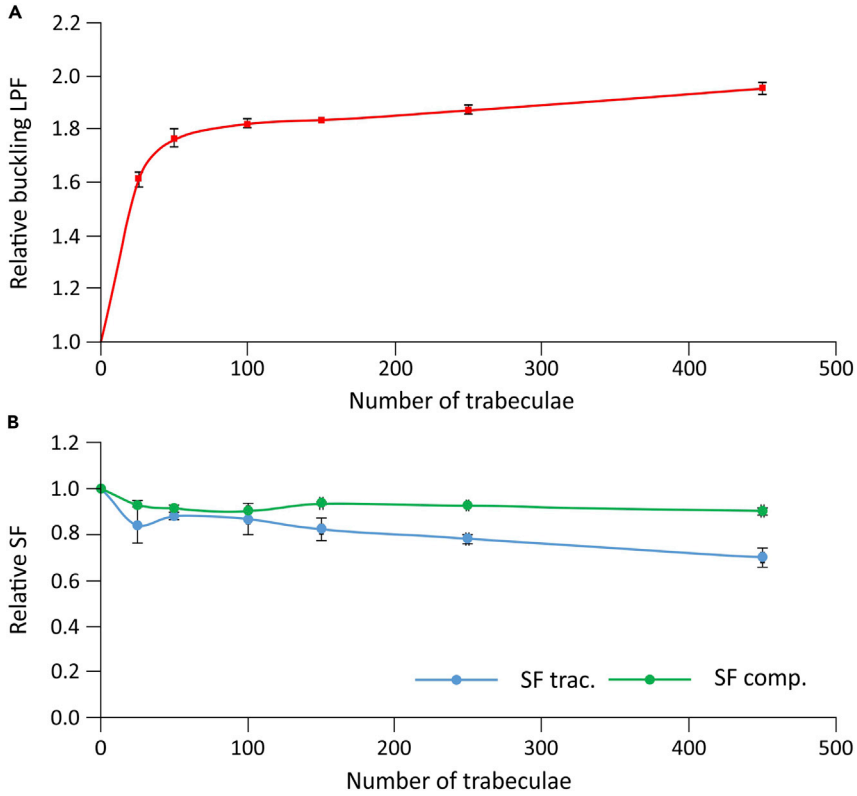

Figure 3. Graphs displaying relative buckling and relative safety factor for a simplified azhdarchid cervical vertebra modeled with varying numbers of trabeculae

(A) Relative increase of buckling load proportional factor (LPF) versus number of trabeculae (average values and standard deviation).

(B) Safety factor (SF) in tension and in compression determined via a static analysis (average values reported) averaged values rated to the no trabeculae condition. The safety factor refers to the strain level. When the number of the trabeculae increases, it increases the mechanical bonding between the external shell of the vertebra and the internal channel; this introduces an increased stress concentration (and therefore strain level) onto the wall of the internal neural tube. In fact, the internal neural tube is the area where stresses and strains are highest, as shown in Figure 4.

non-linearly with the number of trabeculae arranged onto the vertebral body. In particular, the overall trend is of a progressive deterioration of the safety factor in both tension and compression. For all the analyzed cases, the decay in the safety factor is overall within approximately 20% of the initial value. This change is not uniform in both trend and magnitude; a monotonic trend appears only after the level of 150 trabeculae.

Implications for azhdarchid feeding

It has been widely assumed that azhdarchids were either piscivores or generalist feeders taking perhaps small mammals and reptiles (Witton and Naish, 2008). Alternative feeding strategies have been proposed, including skim feeding for surface plankton and probe feeding for molluscs and infaunal arthropods (Lehman and Langston, 1996; Bestwick et al., 2018). There seems to be a consensus that small tetrapods and fish were the likely prey (Averianov, 2013). Thus, based on the structural constraints imposed by the cervical vertebrae, it is pertinent to ask the question, what is a reasonable maximum prey animal mass the pterosaurs were able to catch, lift (with its head and neck), and process?

Adopting for the variables in Equation (5) the values reported above and assuming the elastic modulus for the bone ranging from 15 GPa to 22 GPa, the corresponding maximum mass of the prey ranges between 18 kg and 27 kg. In order to consider dynamical effects related to the flying dynamics and to an expected

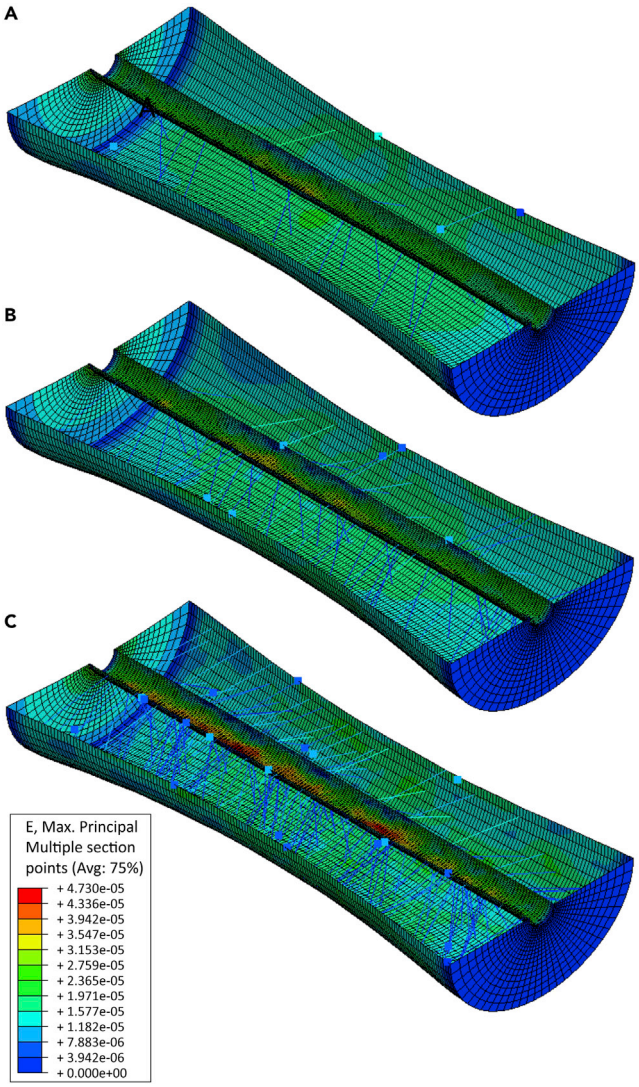

Figure 4. Distribution of the maximum principal strain on the finite element (FE) model; a cross-section showing the effect of the load transfer via the trabeculae

(A–C) (A) 50 trabeculae; (B) 150 trabeculae (optimum number), and (C) 450 trabeculae.

fast action of prey catching, the values related to both the head mass and the prey mass should be multiplied by a magnification factor MF. Equation (5) then becomes:

$$F_p = \frac{1}{MF}\varepsilon_t \frac{JE_b}{L\frac{D_{out}}{2}}\left(\frac{1}{2}qL^2 + MF\,F_h\right). \quad \text{(Equation 6)}$$

In the absence of detailed information about pterosaur feeding strategies, it is hard to identify a reliable value for this load multiplier. Nonetheless, it appears reasonable to consider the same value of the dynamic amplification factor associated with a dynamic system with a suddenly applied load, i.e., 2 (Chao et al., 2020). In this condition, Equation (6) gives a maximum mass for the prey ranging between 9 kg and 13 kg.

DISCUSSION

Previous analyses

Averianov (2013) was first to attempt a biomechanical analysis of the neck of azhdarchid pterosaurs, determining that the neck was held outstretched in a sub-horizontal pose (not straight) and was somewhat "S" shaped at the posterior-most four cervical vertebrae, although the degree of flexion between vertebrae

was no more than 20°. Averianov (2013) considered azhdarchids essentially volant animals feeding on the wing.

Later biomechanical models to determine the "strength" of the azhdarchid neck assumed each vertebra to represent a simple hollow tube (Witton and Habib, 2010: Naish and Witton, 2017). Adoption of a hollow tube proxy is not unreasonable but fails to recognize the role of some of the complexities seen on the external surface and ignores entirely the internal architecture of the vertebrae.

Naish and Witton (2017) concluded that the azhdarchid *Hatzegopteryx* neck vertebrae are substantially stronger than those of *Arambourgiania*, with relative failure forces (RFFs) of 5.26 and 0.38 in coronal plane, respectively when loaded by 2,452 N. They suggested that the relatively thick wall of the vertebrae of *Hatzegopteryx* enhanced buckling strength without altering bending strength. They acknowledged that other internal features also needed to be considered—camellate bone and trabeculae. However, these features were not considered in their analyses. They concluded that *Hatzegopteryx* was a robust form of azhdarchid, whereas *Arambourgiania* was more gracile, occupying distinct ecological niches and perhaps diets. Unfortunately, the comparison is flawed, as the two vertebrae compared are from different parts of the cervical series (Naish and Witton, 2017) and likely would have distinct biomechanical properties in any case.

Vertebral internal architecture

The functional capabilities for any bone result from the combination/interaction of all its structural components. Thus, the internal structure as well as the external components and their mechanical properties must be considered in any analysis of its form and function. This can be extended to its histology, microstructure, and even molecular composition of the bone material itself (e.g., Huiskes, 2000; Rayfield, 2007). XCT scanning revealed an internal structure of a generally thin-walled cylindrical vertebra dominated internally by an axially located bony neural tube supported by a cross-helical arrangement of thin trabeculae along the entire length of the vertebral cylinder.

Additional resistance to buckling could have been achieved by thickening the external walls of the vertebral body; however, such thickening would considerably increase the mass of the vertebra, something that is detrimental for a flying vertebrate. The evolution of a spirally arranged system of thin trabeculae as an alternative allowed for a reduced wall thickness and thus a reduction in the mass of the vertebra along with increased resistance to torsion and compression, i.e., the system was both lighter and stronger and energetically cheaper to construct.

Biomechanical properties of a single vertebra

Our results identify a crucial role of the trabeculae in stabilizing the vertebral structure. As soon as the internal space is populated with trabeculae radially arranged between the neural tube and the external wall, the structure's capability to sustain loads increases; the non-linear nature of this change seems to suggest the existence of an optimal number (approximately 150 trabeculae) of trabeculae able to bring the most relevant benefit to the structural stability without impacting on both mass and stress distribution. When the number of trabeculae increases, the structure is increasingly more stable. Meanwhile, the mechanical connection between the external wall and the internal neural tube also increases. This linkage is responsible for the stabilization process, which is mediated by radial trabeculae: when the number of trabeculae increases, the wall of the internal neural tube is subjected to an increased level of strain (Figure 4). As the stabilization induced by the trabeculae is non-linearly dependent on the number of trabeculae, the increase in stress on the neural tube is also non-linear. The increased level of strain reduces the safety of the structure with respect to any local fracture. Nonetheless, the numerical models suggest this change in the safety factor is marginal and does not change significantly when the number of trabeculae increases.

The numerical analyses provide an insight into the role of the internal bone structure and specifically the role of trabeculae that extend the load-bearing ability by stabilizing the structure without making it significantly heavier. This enhances the mechanical performance of the vertebral structure, preserving its biological integrity while increasing the magnitude of the force that can be applied to a bone segment. These characteristics are of key importance for a predatory flying animal equipped with a long neck used as the main tool to capture and lift prey.

This model may also explain the radial arrangement of the trabecular structure. Although some limited areas of a more isotropic spongy bone can be envisaged locally, the most relevant part of the trabecular structure is distinct from that of the spongy bone of a typical mammalian vertebra, where trabeculae appear predominantly aligned with the vertebral axis. One possible explanation, corroborated by the above-discussed analysis, is related to the extremely slender nature of the vertebral body geometry. The particular combination of aspect ratio and wall thicknesses suggests buckling as the most relevant critical scenario to produce bone fracture. Thus, it is possible that the evolutionary process encouraged and drove the specialization of a trabecular structure able to mitigate as much as possible the risk of buckling instability. If so, this would be in the direction of an optimization process where the maximum load-bearing ability of the skeleton is increased without impacting on the overall mass.

Azhdarchid necks

Hyper-elongate necks are unusual in tetrapods outside of Dinosauria, and animals that possess them are highly distinctive. *Giraffa* and *Tannystropheus* (Nosotti, 2007; Badlangana et al., 2009; Rieppel et al., 2010) are two examples where hyper-elongation involved lengthening of the individual vertebrae rather than an increase in cervical number (Nosotti, 2007; Rieppel et al., 2010), as occurred in plesiosaurs and many avians (some animals, notably sauropod dinosaurs, achieved hyper-elongate necks by adopting both approaches) (O'Keefe and Hiller, 2006; Christian and Dzemski, 2007; Taylor and Wedel, 2013).

In animals with long necks the structure functions either as a mast (brachiosaurid dinosaurs, giraffe, ostrich) raising the head significantly above the ground or as a beam, extending the neck forwards and perhaps laterally also (Martin et al., 1998) (e.g., diplodocid sauropods, plesiosaurs, *Tannystropheus*, and azhdarchid pterosaurs perhaps) (Martin et al., 1998; Nosotti, 2007; Badlangana et al., 2009; Averianov, 2013; Noè et al., 2017). In those animals where the neck functions as a mast the animal is not obliged to feed in the trees as do giraffes. Ostriches are largely ground-feeding birds (Folch, 1992), whereas swans use their long necks to garner food from deeper water than their short-necked cousins, the ducks. The modus operandi of the elongate azhdarchid neck has for a long time been problematic. The analysis of Averianov (2013) showed only limited flexibility in the neck of azhdarchids, whereas Naish and Witton (2017) suggested that it had very limited resistance to buckling.

In those azhdarchids where the head and neck skeleton is known (*Quetzalcoatlus*, *Zhejiangopterus*) the skull is proportionally large (perhaps as long as >1 m for a neck 3 m in length) (Kellner and Langston, 1996; Naish and Witton, 2017), a morphology not seen in any other animal except birds such as pelicans and storks. Such a morphology poses questions for diet and mode of feeding in azhdarchid pterosaurs. A stork-like feeding strategy of terrestrial foraging (Witton and Naish, 2008) and a probe-feeding mode of foraging were proposed for *Quetzalcoatlus*, although the latter hypothesis was based solely on the association of invertebrate trace fossils, rather than any biomechanical analysis (Lehman and Langston, 1996).

Size of prey?

Our analysis allows us to speculate on the maximum mass of prey compatible with the average bony structure identified in the neck of the pterosaur. The limiting factor considered was the prey mass at which the bone component of the vertebrae would fail. We cannot factor in the complexity of the intervertebral joints, connective tissue, and neck musculature, as these remain unknown for Pterosauria. This analysis, based on a simplified cantilever continuous beam model, is affected by many limitations: (1) a static model was assumed; (2) the neck was assumed as a homogeneous structure where only the bony structure is reacting to loads (i.e. the muscular and connective tissue contributions in loading tensional stresses are neglected); (3) either material properties (i.e. density and elastic modulus) or failure criteria for the bone tissue were assumed matching those usually valid for bird bone; and (4) the model assumed for each vertebra was extremely simplified in both the overall geometry and the internal structure. On the other hand, the model appears to be simple and parametric, able to assess the impact of the uncertainties associated with each one of its parameters in a straightforward and clear way. The absence of detailed information about the muscular structure and the flight dynamics would make pointless the elaboration of more complex models involving a more accurate skeletal structure for the purposes of a first rough assessment aimed to identify mostly the order of magnitude of the prey mass.

The values this model produced (9-13 kg) appear reasonable when correlated with the assessed total mass of the animal with a mass estimated to be between ~16 kg and 37 kg for a wingspan of approximately 6 m (Humphries et al., 2007; Witton, 2008).

Concluding remarks

XCT imaging of an azhdarchid pterosaur cervical vertebra reveals a complex internal architecture of radial, spoke-like support structures maintaining the integrity of a centrally located bony neural tube through which passed the main spinal cord. Linear elastic static analysis and linearized buckling analysis reveal that as few as 50 trabeculae increases the buckling load by up to 90%, implying that a cervical vertebra without the trabeculae is considerably more prone to elastic instability due to axial loads. Subsuming the neural tube into the centrum tube and supporting it with an optimum number of fine-spoke-like trabeculae adds considerable resistance to buckling to the cervical series, potentially permitting the uptake of heavy prey items without risking damage to the cervical skeleton, while at the same time without significant mass increase of the skeleton. Calculations applied to the entire neck indicate a prey size lift capability without failure of between 9 kg and 13 kg. Our results are consistent with large prey capture by azhdarchids, including giant forms like *Quetzalcoatlus*, with a wingspan of 10 m or more (Lawson, 1975). Prey size was likely limited by skull and gullet size, rather than neck lifting capacity. We also acknowledge that the neck strength may have been utilized for another function, such as neck "bashing," an inter-male rivalry behavior seen in giraffes. Alternatively, the seemingly overengineered cervical vertebrae could be related to shearing forces associated with large skulls being buffeted by strong winds during flight or while on the ground.

Limitations of the study

Despite their popular appeal, azhdarchid pterosaurs are poorly understood. Their remains are incredibly rare, mostly fragmentary and usually crushed. The cervical vertebral series is only known for three taxa, *Phosphatodraco*, *Zhejiangopterus*, and *Quetzalcoatlus*, all of which are crushed to varying degrees. The specimen described here is remarkable for its 3-dimensionality with internal structure intact and is almost unique.

The model assumed for each vertebra was highly simplified in both the overall geometry and the internal structure. A hollow cylinder within a hollow cylinder mimics the overall structure of the living system. We did not consider the complexities of the articulatory surfaces, processes, and structural features at the anterior and posterior terminations of the vertebra. Similarly, our mass calculations are based on a simplified model of the vertebra.

Our mathematical analysis is based on a cantilever continuous beam model affected by several limitations: (1) a static model was assumed; (2) the neck was assumed as a homogeneous structure where only the bony structure is reacting to loads (i.e. the muscular and connective tissue contributions in loading tensional stresses are disregarded); (3) either material properties (i.e. density and elastic modulus) or failure criteria for the bone tissue were assumed to match those valid for bird bone.

Resource availability

Lead contact

Further information and requests for resources should be directed to and will be fulfilled by the lead contact, Miss Cariad J. Williams, cariad.williams1996@gmail.com.

Material availability

The original specimen is accessioned in the collection of FSAC. Digital scans and videos are available on request. The thin section of Figure S1 is accessioned in the collection of the SEGG, University of Portsmouth, UK.

Data and code availability

All data are included in this submission.

METHODS

All methods can be found in the accompanying transparent methods supplemental file.

SUPPLEMENTAL INFORMATION

Supplemental information can be found online at https://doi.org/10.1016/j.isci.2021.102338.

ACKNOWLEDGMENTS

We are grateful to Mr Ian Eaves, London for allowing us unlimited access to his collection of pterosaurs and for the facility to create 3D replicas of his specimens from the Kem Kem Group. We thank Dr Samir Zouhri for assistance with fieldwork in Morocco. We thank two anonymous referees and Liz Martin-Silverstone and Colin Palmer for their incredibly helpful commentary.

AUTHOR CONTRIBUTIONS

C.J.W., data gathering, 3D modeling, writing MS, visualizations. M.P., mathematical modeling, data processing, writing MS. A.B., mathematical modeling, data processing, writing MS. R.E.S., fieldwork, data processing, writing MS. A.K., XCT scanning and data processing, writing MS. W.K., topographic scanning, data processing, 3D printing, writing MS, visualizations. N.I., fieldwork, writing MS. D.M.M., conceptualization, fieldwork, supervision, writing MS.

DECLARATION OF INTERESTS

The authors declare no conflicts of interest.

Received: August 9, 2020
Revised: February 10, 2021
Accepted: March 17, 2021
Published: April 14, 2021

REFERENCES

Averianov, A.O. (2010). The osteology of *Azhdarcho lancicollis* nessov, 1984 (pterosauria, Azhdarchidae) from the late cretaceous of Uzbekistan. Proc. Zool. Inst. RAS *314*, 264–317.

Averianov, A.O. (2013). Reconstruction of the neck of *Azhdarcho lancicollis* and lifestyle of azhdarchids (Pterosauria, Azhdarchidae). Paleontol. J. *47*, 203–209.

Badlangana, N.L., Adams, J.W., and Manger, P.R. (2009). The giraffe (*Giraffa camelopardalis*) cervical vertebral column: a heuristic example in understanding evolutionary processes? Zool. J. Linn. Soc. *155*, 736–757.

Bennett, S.C. (1997). The arboreal leaping theory of the origin of pterosaur flight. Hist. Biol. *12*, 265–290.

Bennett, S.C. (2014). A new specimen of the pterosaur *Scaphognathus crassirostris*, with comments on constraint of cervical vertebrae number in pterosaurs. Neues Jahrb. Geol. Paläontol. *271*, 327–348.

Bestwick, J., Unwin, D.M., Butler, R.J., Henderson, D.M., and Purnell, M.A. (2018). Pterosaur dietary hypotheses: a review of ideas and approaches. Biol. Rev. *93*, 2021–2048, https://doi.org/10.1111/brv.12431.

Buffetaut, E., Grigorescu, D., and Csiki, Z. (2003). Giant azhdarchid pterosaurs from the terminal Cretaceous of Transylvania (western Romania). Geol. Soc. Spec. Publ. *217*, 91–104.

Buffetaut, E., and Kuang, X. (2010). The tuba vertebralis in Dsungaripterid pterosaurs. Acta Geosci. Sin. *31*, 10–11.

Butler, R.J., Barrett, P.M., and Gower, D.J. (2009). Postcranial skeletal pneumaticity and air-sacs in the earliest pterosaurs. Biol. Lett. *1*, 1–4.

Chao, Z., Hong, H., Kaiming, B., and Xueyuan, Y. (2020). Dynamic amplification factors for a system with multiple degrees of freedom. Earthq. Eng. Eng. Vib. *19*, 363–375, https://doi.org/10.1007/s11803-020-0567-9.

Christian, A., and Dzemski, G. (2007). Reconstruction of the cervical skeleton posture of *Brachiosaurus brancai* Janensch, 1914 by an analysis of the intervertebral stress along the neck and a comparison with the results of different approaches. Foss. Rec. *10*, 38–49.

Claessens, L.P.A.M., O'Connor, P.M., and Unwin, D.M. (2009). Respiratory evolution facilitated the origin of pterosaur flight and aerial gigantism. PLoS One *4*, e4497, https://doi.org/10.1371/journal.pone.0004497.

Company, J., Ruiz-Omeñaca, J.I., and Suberbiola, X.P. (1999). A long-necked pterosaur (pterodactyloidea, Azhdarchidae) from the upper cretaceous of valencia, Spain. Geol. Mijnbouw *78*, 319–333.

Dumont, E.R. (2010). Bone density and the lightweight skeletons of birds. Proc. R. Soc. B *277*, 2193–2198.

Folch, A. (1992). Order struthioformes. In Handbook of the Birds of the World 1, J. del Hoyo, A. Elliott, and J. Sargatal, eds. (Lynx Edicions), pp. 11–761.

Frey, E., and Martill, D.M. (1996). A reappraisal of *Arambourgiania* (Pterosauria, Pterodactyloidea): one of the world's largest flying animals. Neues Jahrb. Geol. Paläontol. Abh. *199*, 221–247.

Harrell, T.L., Jr., Gibson, M.A., and Langston, W., Jr. (2016). A cervical vertebra of *Arambourgiania philadelphiae* (pterosauria, Azhdarchidae) from the late campanian micaceous facies of the coon creek formation in McNairy county, Tennessee, USA. Bull. Am. Mus. Nat. Hist. *33*, 94–103.

Henderson, M.D., and Peterson, J.E. (2006). An azhdarchid pterosaur cervical vertebra from the Hell Creek Formation (Maastrichtian) of southeastern Montana. J. Vertebr. Paleontol. *26*, 192–195.

Howse, S.C.B. (1986). On the cervical vertebrae of the pterodactyloidea (reptilia: archosauria). Zool. J. Linn. Soc. *88*, 307–328.

Huiskes, R. (2000). If bone is the answer, then what is the question? J. Anat. *197*, 145–156.

Humphries, S., Bonser, R.H.C., Witton, M.P., and Martill, D.M. (2007). Did pterosaurs feed by skimming? Physical modelling and anatomical evaluation of an unusual feeding method. PLoS Biol. *5*, e204, https://doi.org/10.1371/journal.pbio.0050204.

Ibrahim, N., Sereno, P.C., Varricchio, D.J., Martill, D.M., Dutheil, D.B., Unwin, D.M., Baidder, L., Larsson, H.C., Zouhri, S., and Kaoukaya, A. (2020). Geology and paleontology of the upper cretaceous Kem Kem group of eastern Morocco. ZooKeys *928*, 1–216.

Ibrahim, N., Unwin, D.M., Martill, D.M., Baidder, L., and Zouhri, S. (2010). A new pterosaur (pterodactyloidea: Azhdarchidae) from the upper cretaceous of Morocco. PLoS One *5*, e10875, https://doi.org/10.1371/journal.pone.0010875.

Kellner, A.W.A., and Langston, W., Jr. (1996). Cranial remains of *Quetzalcoatlus* (pterosauria, Azhdarchidae) from late cretaceous sediments of big bend national park, Texas. J. Vertebr. Paleontol. *16*, 222–231.

Lavocat, R. (1954). Sur les dinosauriens du Continental Intercalaire des Kem-Kem de la Daoura. Comptes Rendus 19th Int. Geol. Congress *1952*, 65–68.

Lawson, D.A. (1975). Pterosaur from the latest Cretaceous of West Texas. Discovery of the largest flying creature. Science *187*, 947–948.

Lehman, T.M., and Langston, W., Jr. (1996). Habitat and behaviour of *Quetzalcoatlus*: paleoenvironmental reconstruction of the javelina formation (upper cretaceous), big bend national park, Texas. J. Vertebr. Paleontol. *16*, 48A.

Liu, D.-X., Zhou, C.-F., Wang, J.-Q., Li, W.-G., and Wei, Q.-W. (2015). New data on the cervical morphology of the Chinese tapejarine. Hist. Biol. *27*, 638–645.

Longrich, N.R., Martill, D.M., and Andres, B. (2018). Late maastrichtian pterosaurs from north africa and mass extinction of pterosauria at the cretaceous-paleogene boundary. Plos Biol. *16*, e2001663.

Martill, D.M., Frey, E., Sadaqah, R.M., and Khoury, H.N. (1998). Discovery of the holotype of the giant pterosaur *Titanopteryx philadelphiae* Arambourg 1959, and the status of *Arambourgiania* and *Quetzalcoatlus*. Neues Jahrb. Geol. Paläontol. Abh. *207*, 57–76.

Martin, J., Martin-Rolland, V., and Frey, E. (1998). Not cranes or masts, but beams: the biomechanics of sauropod necks. Oryctos *1*, 113–120.

Martin, E.G., and Palmer, C. (2014). Air space proportion in pterosaur limb bones using computed tomography and its implications for previous estimates of pneumaticity. PLoS One *9*, e97159, https://doi.org/10.1371/journal.pone.0097159.

Naish, D., and Witton, M.P. (2017). Neck biomechanics indicate that giant Transylvanian azhdarchid pterosaurs were short-necked arch predators. PeerJ *5*, e2908, https://doi.org/10.7717/peerj.2908.

Noè, L.F., Taylor, M.A., and Gómez-Pérez, M. (2017). An integrated approach to understanding the role of the long neck in plesiosaurs. Acta Palaeontol. Pol. *62*, 137–162.

Nosotti, S. (2007). *Tanystropheus longobardicus* (reptilia protorosauria): Re-interpretations of the anatomy based on new specimens from the middle triassic of besano (lombardy, northern Italy). Mem. Soc. Ital. Sci. Nat. Mus. Civ. Stor. Nat. Milano *35*, 1–88.

O'Keefe, F.R., and Hiller, N. (2006). Morphologic and ontogenetic patterns in elasmosaur neck length, with comments on the taxonomic utility of neck length variables. Paludicola *5*, 206–229.

Rayfield, E.J. (2007). Finite element analysis and understanding the biomechanics and evolution of living and fossil organisms. Annu. Rev. Earth Planet. Sci. *35*, 541–576.

de Ricqlès, A.J., Padian, K., Horner, J.R., and Hélène, F.-V. (2000). Palaeohistology of the bones of pterosaurs (Reptilia: archosauria): anatomy, ontogeny, and biomechanical implications. Zool. J. Linn. Soc. *129*, 349–385.

Rieppel, O., Jiang, D.-Y., Fraser, N.C., Hao, W.-C., Motani, R., Sun, Y.-L., and Sun, Z.-Y. (2010). *Tanystropheus* cf. *T. longobardicus* from the early late triassic of guizhou province, southwestern China. J. Vertebr. Paleontol. *30*, 1082–1089.

Sereno, P.C., Dutheil, D.B., Iarochene, M., Larsson, H.C.E., Lyon, G.H., Magwene, P.M., Sidor, C.A., Varricchio, D.J., and Wilson, J.A. (1996). Predatory dinosaurs from the sahara and late cretaceous faunal differentiation. Science *272*, 986–991.

Steel, L. (2008). The palaeohistology of pterosaur bone: an overview. Zitteliana *B28*, 109–125.

Taylor, M.P., and Wedel, M.J. (2013). Why sauropods had long necks; and why giraffes have short necks. PeerJ *1*, e36, https://doi.org/10.7717/peerj.36.

Unwin, D.M. (2003). On the phylogeny and evolutionary history of pterosaurs. Geol. Soc. Spec. Publ. *217*, 139–190.

Unwin, D.M. (2005). The Pterosaurs from Deep Time (Pi Press).

Unwin, D.M., and Lü, J. (1997). On *Zhejiangopterus* and the relationships of pterodactyloid pterosaurs. Hist. Biol. *12*, 199–210.

Vremir, M., Witton, M., Naish, D., Dyke, G., Brusatte, S.L., Norell, M., and Totoianu, R. (2015). A medium-sized robust-necked azhdarchid pterosaur (pterodactyloidea: Azhdarchidae) from the maastrichtian of pui (haţeg basin, transylvania, Romania). Am. Mus. Novit. 1–16.

Watabe, M., Tsuihiji, T., Suzuki, S., and Tsogtbaatar, K. (2009). The first discovery of pterosaurs from the Upper Cretaceous of Mongolia. Acta Palaeontol. Pol. *54*, 231–242.

Wellnhofer, P. (1991). Additional pterosaur remains from the santana formation (aptian) of the chapada do araripe, Brazil. Palaeontogr. Abt. A. *215*, 43–101.

Witton, M.P. (2008). A new approach to determining pterosaur body mass and its implications for pterosaur flight. Zitteliana *28*, 143–158.

Witton, M.P. (2013). Pterosaurs: Natural History, Evolution, Anatomy (Princeton University Press).

Witton, M.P., and Habib, M.B. (2010). On the size and flight diversity of giant pterosaurs, the use of birds as pterosaur analogues and comments on pterosaur flightlessness. PLoS One *5*, e13982.

Witton, M.P., and Naish, D. (2008). A reappraisal of azhdarchid pterosaur functional morphology and paleoecology. PLoS One *3*, e2271.

iScience, Volume *24*

Supplemental information

Helically arranged cross struts in azhdarchid pterosaur cervical vertebrae and their biomechanical implications

Cariad J. Williams, Martino Pani, Andrea Bucchi, Roy E. Smith, Alexander Kao, William Keeble, Nizar Ibrahim, and David M. Martill

Transparent Methods

The pterosaur cervical vertebra analysed here is provisionally identified as *Alanqa* sp. on the basis that 1, it has an azhdarchid construction, and 2, it is found in a taphocoenosis with jaws confidently identified as *Alanqa saharica*. There is little doubt that the specimen is from an azhdarchid, but its precise generic and specific identity can only be provisional. The specimen (Main Text Figure 1) FSAC KK 5077, was obtained from Aferdou N'Chaft, near the oasis of Hassi El Begaa in the Tafilalt of south east Morocco and is accessioned in the collection of the Faculté des Sciences Aïn Chock, Université Hassan II, Casablanca, Morocco. Specimens from Begaa occur in a thin (0 mm-~500 mm) mud-flake conglomerate within the Ifezouane Formation of the Kem Kem Group (Martill et al., 2018; Ibrahim et al., 2020). Bones from this horizon are usually isolated and may be broken, but some elements are in near perfect condition. Preservation of the bone microstructure is also excellent (see Figure S1). Three-dimensional prints from the XCT scans of the specimen are accessioned in the collection of the University of Portsmouth School of the Environment, Geography and Geosciences (UOP-PAL-KK 007).

XCT scanning. X-ray computed tomography (XCT) was conducted using an X-ray microscope (Xradia 520 Versa, Carl Zeiss X-ray Microscopy, located at the University of Portsmouth) operating at a voltage of 80 kVp with a power of 6 W and a tube current of 75 µA. A ZEISS LE1 proprietary filter positioned directly after the X-ray source filtered the X-ray spectrum. A tomography was collected using a flat panel detector to acquire 1601 projection images over 360 degrees with an interval of 0.22 degrees. The detector was exposed for 0.5 seconds (5 frames, 0.1 s exposure/frame) for each projection. The voxel size of the scans is 69.4 µm. The projections were reconstructed using the microscope software, incorporating a filtered back projection algorithm (Scout and Scan Reconstructor, Carl Zeiss Microscopy). For each dataset the centre shift was manually found, no beam hardening correction was utilised and a smoothing correction of 0.5 applied.

XCT data manipulation. MeVisLab software was used to digitally remove the matrix of the CT scanned specimen to observe the internal structure. GeoMagic Design X was used to generate sections and 3-D images of the scanned vertebra. Three-dimensional models were printed from the scans of the original specimen and accessioned as UOP-PAL-KK 007 from this data (see above).

Numerical modelling. The geometry of the pterosaur cervical vertebra has been parametrically generated in Matlab and then analysed in ABAQUS. The idealised geometry is summarised in Figure S2, where key reference parameters are reported using the notation adopted below. The vertebra is modelled as a hyperboloid with elliptical cross-section with an eccentricity of 0.6. The elliptical section at the top and bottom has major axis D_M = 60mm and minor axis D_m= 48 mm, the minimal elliptical section, located at the middle of the vertebra has D_M = 46 mm and D_m = 36.8 mm), the overall vertebra length L = 160 mm and wall thickness t = 1 mm. The geometry has been analysed via 21480 S4 shell elements, a four nodes quadrilateral linear element. The exterior surface used 9600 elements (60 elements in the circumferential direction and 160 elements in the axial direction). The neural canal was modelled as a hollow cylinder (length L = 160 mm, radius R = 4 mm, wall thickness 0.7 mm) and it was meshed with 9600 S4 shell elements (60 divisions along the circumference and 160 divisions along the longitudinal axis). The resulting hollow geometry was then closed by top and bottom shell caps with a thickness of 12 mm, each discretized with 1140 S4 shell elements. Mesh details are represented in Figure S3A. The dimensions used were taken directly from the XCT scans and reflect as near as possible those of the original specimen.

Linear elastic static analyses as well as linearised buckling analyses were performed. The bone was considered as a linear elastic material with a Young's modulus E = 22 GPa and Poisson ratio ν = 0.3. Trabeculae connecting the inner neural canal radially to the external vertebral walls were randomly generated and distributed along the longitudinal axis. The number of trabeculae has been assumed as a parameter in the numerical analysis and varied in the range (0-450) to assess their effect on the mechanical behaviour of the structure. All the trabeculae were assigned the same radius (R_{trab} = 0.5 mm) but they had a different length: in fact, each trabecula was generated by randomly connecting

nodes on the neural tube walls with nodes on the external wall of the vertebra; the algorithm for defining the trabeculae was designed for producing sub-radial elements (i.e. small deviations from a perfectly radial direction were allowed). The overall arrangement looks like the distribution of the spokes on a bicycle wheel. Trabeculae were modelled as B31 beam elements, a two nodes linear element, that assumes the beam is shear deformable as per Timoshenko beam theory. See Figure S3B.

As boundary conditions, all nodes placed at the bottom surface were fully constrained; a uniformly distributed compression load was applied on the top lid with a reference magnitude of 100 kPa. This fictitious load is then multiplied by the Load Proportional Factor (LPF) resulting from the stability analysis to assess the ultimate load which the structure can bear before the onset of an elastic instability (i.e., buckling).

In order to elucidate the impact of the trabeculae on the mechanics of the vertebra, seven different conditions were considered corresponding to seven distinct number of randomly generated trabeculae (i.e. 0, 25, 50, 150, 250 and 450 trabeculae); to take into account possible local effects related to the randomised nature of both distribution and positioning of the trabeculae, three models were created for each trabecular numerosity.

The mechanical behaviour was analysed with respect to two failure scenarios: structural instability and material fracture. The structural stability was assessed by analysing linear buckling induced by the axial load; the load multiplier associated to the first instability mode was calculated for each model. Material fracture was analysed by means of static analysis: A strain-based failure criterion asymmetric for tension and compression, commonly considered for describing bone failure (Nalla et al., 2003; Schileo et al., 2008), was adopted; for each model: the bone was assumed to fail when the principal strain value in compression and in tension reached 1.1% and 0.8% respectively. The safety factor with respect to the material collapse was calculated as the ratio between the critical strain value in compression/tension and the actual value of the maximum principal strain in compression/tension.

Determining biomechanical properties of the neck. The neck of the animal was considered as a cantilever continuous beam **L** = 1.2 m long, comprising a sequence of nine contiguous vertebrae; the average vertebra was described as a can (hollow cylinder) model with the following geometry:

- length (**Lv**) = 0.14 m
- Outer diameter (**Dout**) = 0.05 m
- Inner diameter (**Din**) = 0.048 m

The resulting cross section was then a circular crown (area = $15.39*10^{(-5)}$ m^2, second moment with respect to a principal axis of inertia **I** = $4.6*10^{(-8)}$ m^4). The volume of the bone tissue (**Vb**) of each vertebra = $21.55*10^{(-6)}$ m^3, the corresponding bone marrow volume (**Vm**) = $12.67*10^{(-5)}$ m^3. The neck was modelled as a cantilever continuous beam subjected to simple bending resulting from three loads:

A. The distributed load (**q**) related to the mass of the neck.
B. The concentrated load (**Fh**) associated with the mass of the animal's head**.**
C. The concentrated weight associated to the mass of the prey (**Fp**).

The weight of the neck was assessed by considering the mass of both bone tissue (volumetric mass = 2000 kg/m^3) and bone marrow (volumetric mass = 1000 kg/m^3) for each vertebra (Currey, 2002). The internal cavity was assumed to be filled with bone marrow only for half of the internal volume, as this is an unknown for pterosaur pneumatised bones. Therefore, the mass of the single vertebra was $\mathbf{m_v}$ = 0.168 kg, as a fraction of the overall cantilever model, corresponding to a uniformly distributed load **q** = 10.41 N/m. The bending moment ($\mathbf{M_{tot}}$) at the fully constrained end is then given by:

$$\boldsymbol{M_{tot} = \frac{1}{2} qL^2 + F_h L + F_p L} \qquad (1)$$

Assuming a linear distribution of the stresses on the cross-section area (i.e. a Navier's stress diagram, typical of the simple bending on homogeneous cross sections), the magnitude of the maximum stress in either tension and compression is given by:

$$|\boldsymbol{\sigma_{max}}| = \frac{\boldsymbol{M_{tot}\, D_{out}}}{\boldsymbol{2J}} \qquad (2)$$

The corresponding strain is:

$$\boldsymbol{\varepsilon_{max}} = \frac{|\boldsymbol{\sigma_{max}}|}{\boldsymbol{E_b}} \qquad (3)$$

Where **Eb** is the elastic modulus of the bone tissue. For the bone tissue, a strain-based failure criterion with asymmetric threshold values in tension and compression (εt = 0.8%; εc = 1.1%) was assumed. Combining equations (1), (2) and (3), the maximum weight of the prey is the value of Fp that produces the maximum admissible strain in traction:

$$\boldsymbol{\varepsilon_t} = \frac{\left(\frac{1}{2}\boldsymbol{qL^2} + \boldsymbol{F_h L} + \boldsymbol{F_p L}\right)\frac{\boldsymbol{D_{out}}}{2}}{\boldsymbol{JE_b}} \qquad (4)$$

That gives:

$$\boldsymbol{F_p} = \boldsymbol{\varepsilon_t}\frac{\boldsymbol{JE_b}}{\boldsymbol{L}\frac{\boldsymbol{D_{out}}}{2}} - \left(\frac{1}{2}\boldsymbol{qL^2} + \boldsymbol{F_h}\right). \qquad (5)$$

Supplemental Figures and Table

Parameter	Value in mm
Maximum preserved length	160*
Maximum width across anterior zygapophyses	96**
Maximum preserved centrum height	45***
Maximum posterior width as preserved	59
Anterior height as preserved	39 ***

Table S1. Selected measurement for cervical vertebrae FSAC KK 5077 (see Figure 1). *Measurement excludes posterior zygapophyses as these are missing from the specimen. ** Measured from tip of right anterior zygapophyses multiplied by 2. *** Part of the neural spine is missing, perhaps ~ 10 mm.

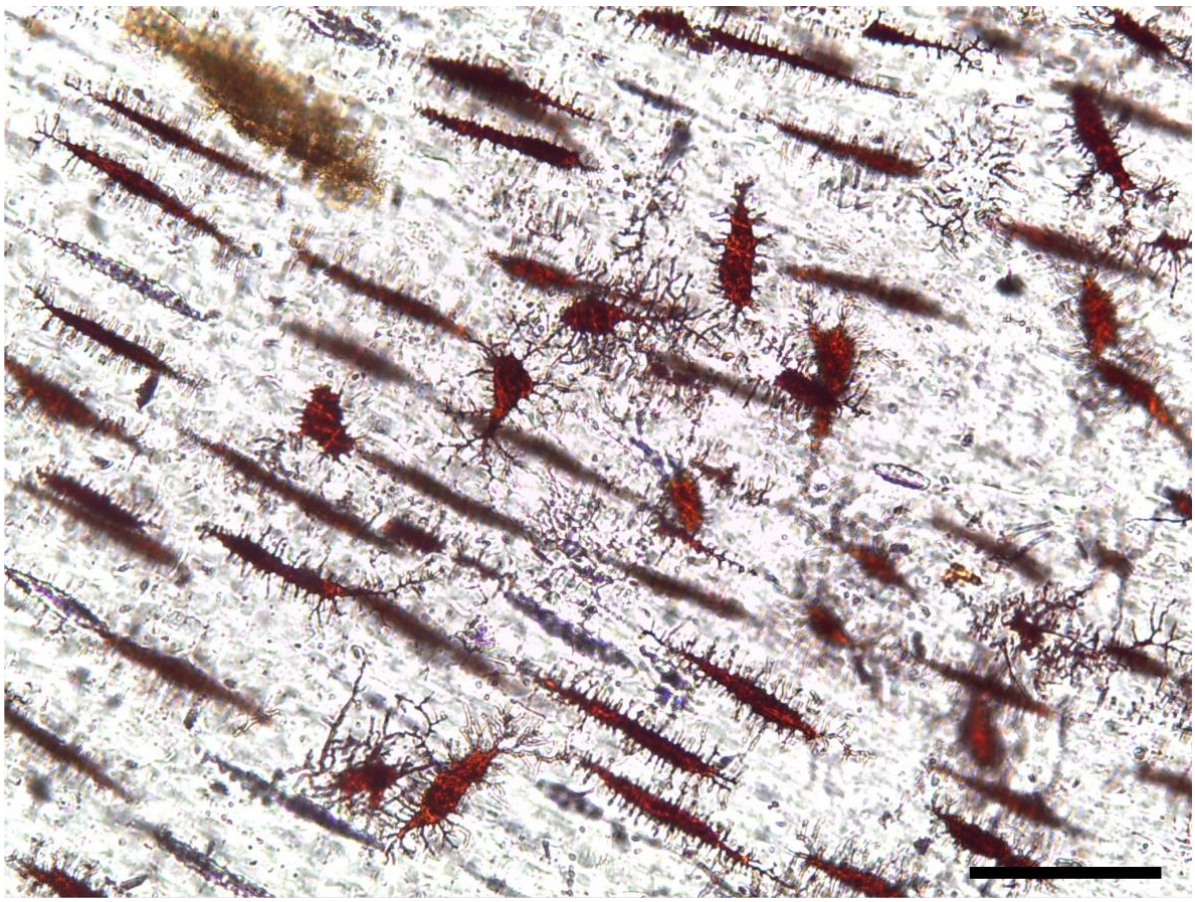

Figure S1. Thin section image of a trabeculae from a pterosaur atlas-axis vertebral complex showing the exceptional preservation of osteocytes and canaliculi. Specimen number UOP-PAL-KK-007. From the same locality as Figure 1. Scale represents 50 µm.

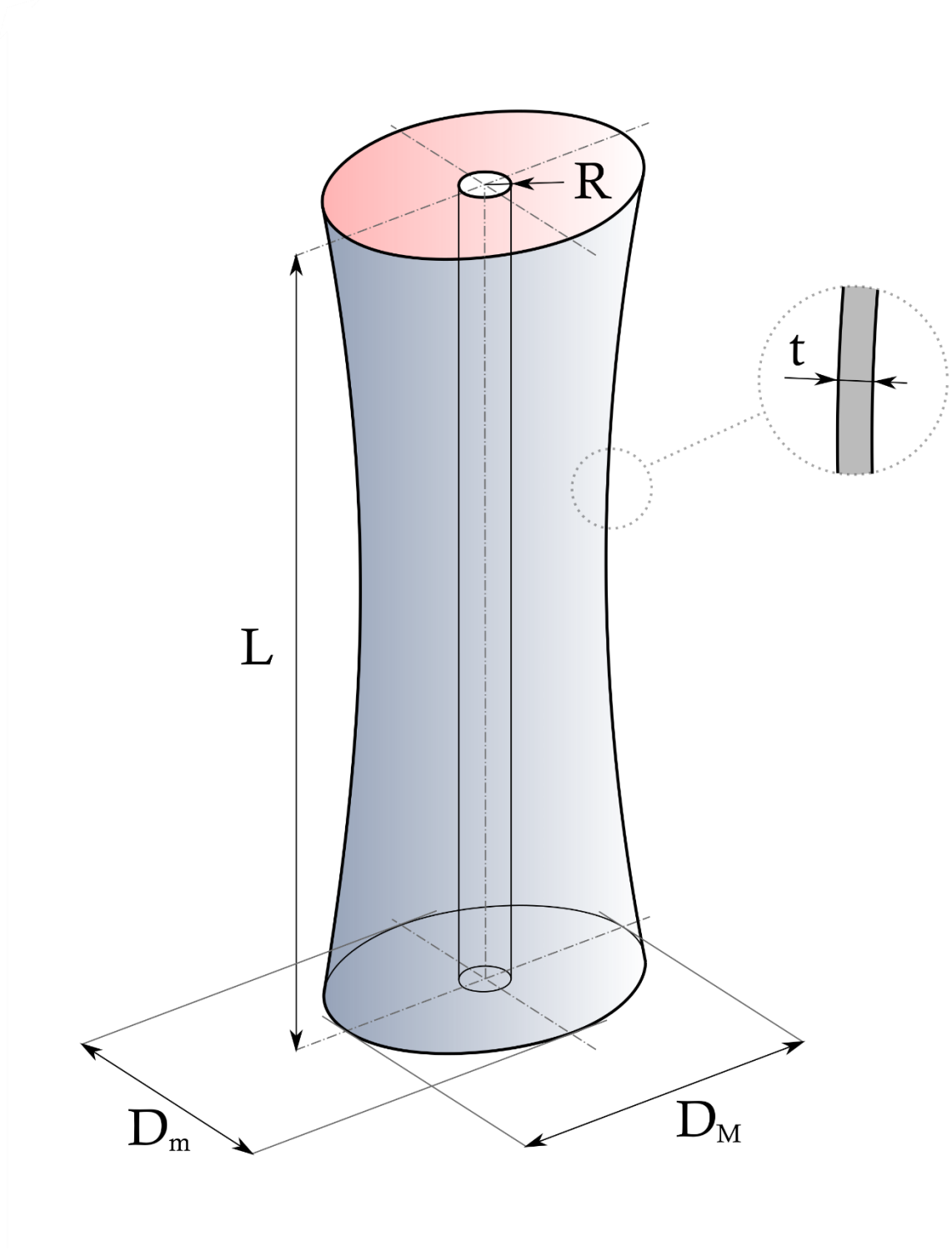

Figure S2. Geometry of the parametric model for the vertebral body. R, radius of neural tube; D_M, larger diameter of centrum; D_m, smaller diameter of centrum; L, length of centrum; t, bone wall thickness. This simplified model is based upon the vertebra in Figure 1.

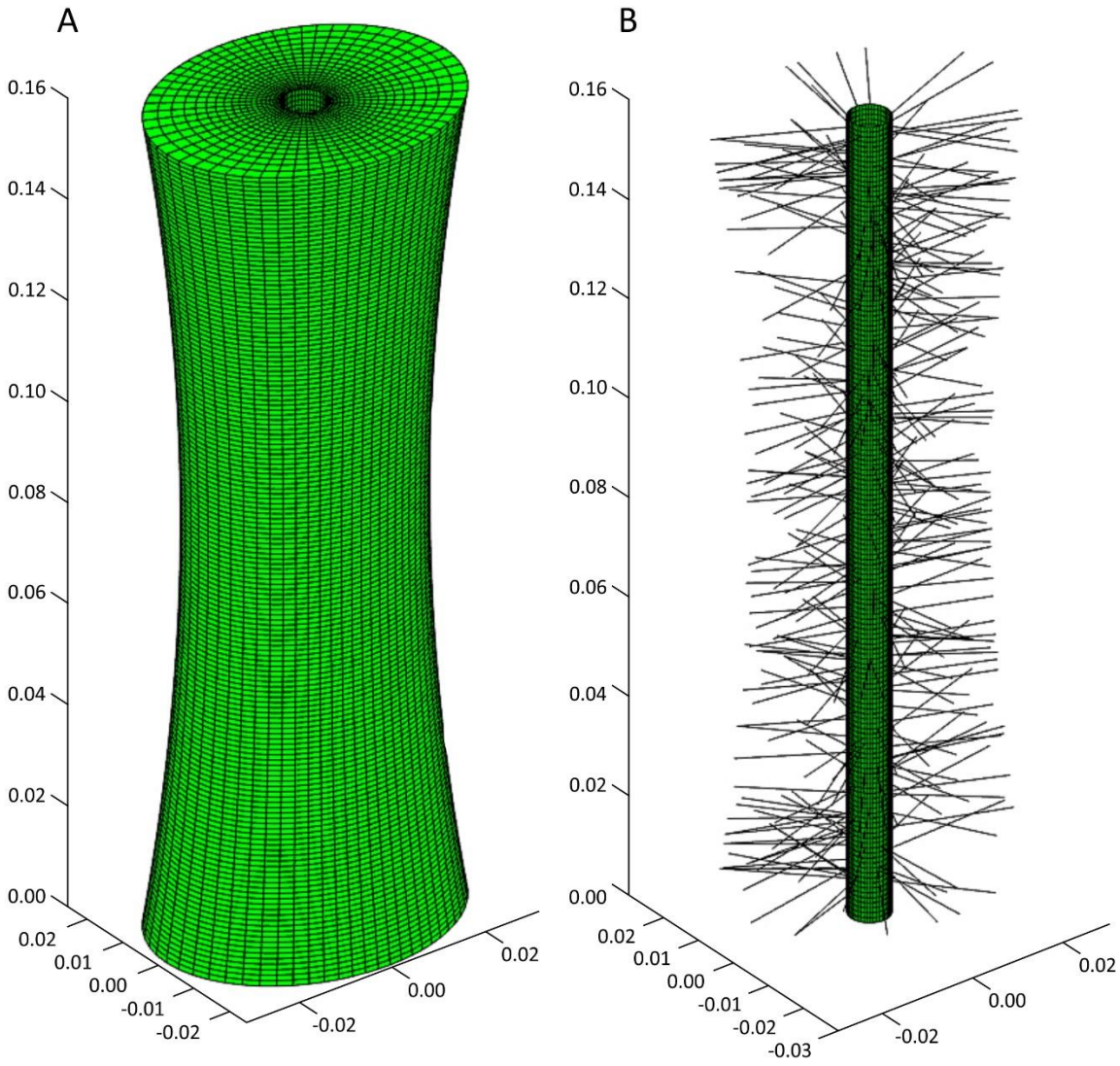

Figure S3. Computational mesh: (A) external wall and top lid; (B) detail of the internal structure: the internal neural tube is connected to the external vertebral wall by radial trabeculae, randomly arranged on the total bone marrow space and producing a “spoke-like” structure. This schematic based on XCT scans of specimen in Figure 1 and seen in Figure 2.

References

Currey J. D. (2002). Bones: structure and mechanics: Princeton University Press, 456 pp.

Ibrahim, N., Sereno, P.C., Varricchio, D.J., Martill, D.M., Dutheil, D.B., Unwin, D.M., Baidder, L., Larsson, H.C., Zouhri, S., and Kaoukaya, A. (2020). Geology and paleontology of the Upper Cretaceous Kem Kem Group of eastern Morocco. ZooKeys *928*, 1-216.

Martill, D.M., Unwin, D.M., Ibrahim, N., and Longrich, N. (2018). A new edentulous pterosaur from the Cretaceous Kem Kem beds of south eastern Morocco. Cretaceous Research *84*, 1-12.

Nalla, R.K., Kinney, J.H., Ritchie, R.O. (2003). Mechanistic fracture criteria for the failure of human cortical bone. Nature Materials *2*, 164-168.

Schileo, E., Taddei, F., Cristofolini, L., Viceconti, M. (2008). Subject-specific finite element models implementing a maximum principal strain criterion are able to estimate failure risk and fracture location on human femurs tested in vitro. Journal of Biomechanics *41*, 356-367. doi:10.1016/j.jbiomech.2007.09.009